

# Application of SMA Composites in the Collectors of the Railway Pantograph for the Italian High-Speed Train

A. Tuissi, P. Bassani, R. Casati, M. Boccione, A. Collina, M. Carnevale, A. Lo Conte, and B. Previtali

(Submitted October 14, 2008; in revised form February 20, 2009)

In high-speed train operation the flexural modes of the collector play a significant role in the vibrations for the frequencies over 40-50 Hz. In a previous work it has been established that a possible way to increase the modal damping of these flexural modes, without deep modification of the collector structure, is to increase the specific damping of the lateral horns, usually made of glass fiber polymer. Ni-Ti alloy yarns can be used as “smart fibers” embedded in this conventional material in order to make new horns with increased damping capacity, with a configuration of laminated composite material. The first step of the work herein presented consists in setting, through a proper thermal treatment, martensitic structure within the pantograph working temperature range, in order to obtain damping capabilities at low amplitude strain in the range  $10^{-4}$ - $10^{-3}$ . Afterwards a series of dynamic tests aimed at identifying the damping capacity of the NiTi wires has been undertaken. A finite element (FE) model of the SMA composites horn has been finally validated, comparing the results of dynamic numerical analysis with the results of measurements.

**Keywords** composite material, damping, shape memory alloy

## 1. Introduction

In high-speed train operation, dynamic behavior of the pantograph heavily influences the quality of current collection. In particular, the flexural modes of the collector play a significant role in the vibrations for the frequencies over 40-50 Hz. In this range, the vibration level is high and consequently high are the levels of sparking and the wear rate of the contact wire and of the contact strip due to electric arcs.

The sources of excitation of these vibrations are mainly two: the direct dynamic interaction of the collector with the contact wire of the overhead line, and the air flow acting on the pantograph. In the latter, both turbulence effects and non-stationary aerodynamic phenomena, in particular, vortex shedding are involved.

The influence of collector deformability has been confirmed through wind tunnel tests, as shown in Fig. 1 where the spectral analysis of the contact force measured during a run-up and run-down test on a complete pantograph is reported. The contribution of the flexural modes of the collector can be clearly

identified at 60 and 137 Hz, corresponding to the first and third flexural modes of vibration of the collector.

In a previous work (Ref 1) it has been established that a possible way to increase the modal damping of the flexural mode of the collectors, without deep modification of collector structure, is to increase the specific damping of the lateral horns, whose primary function is to prevent an irregular positioning of the contact wire with respect to the collector.

Since the material of the lateral horns is usually glass fiber polymer, martensitic Ti-Ni alloy yarns, thanks to the high damping capacity of the NiTi in its martensitic microstructure, can be used as “smart fibers” embedded in this conventional material in order to make new horns with increased damping capacity, with a configuration of laminated composite material like the ones reported in (Ref 2-4).

The first step of the work herein presented consists in the setting of the material structure in order to obtain martensitic phase in the working temperature range through a proper thermal treatment. Afterwards, a series of dynamic tests aimed at identifying the damping properties of the NiTi wires, under uniaxial vibration tests, has been undertaken. The same wires have been used to produce composite SMA prototype.

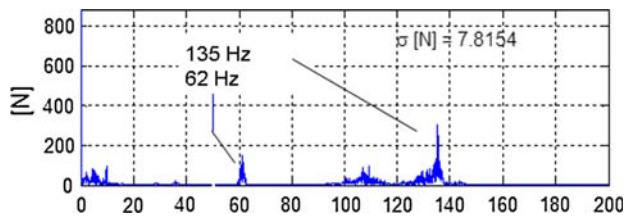
Moreover, a finite element (FE) model of the SMA composites horn has been subsequently validated, comparing the results of dynamic numerical analysis with the results of measurements (Fig. 1).

The paper is organized as follows:

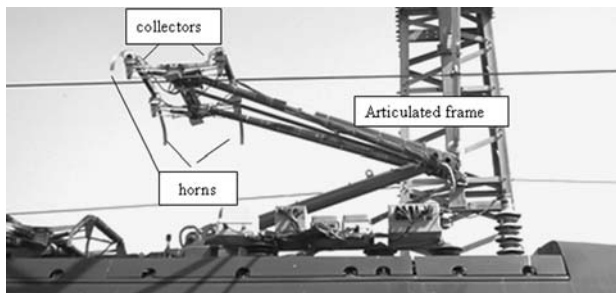
- modal analysis of a current collector by means of testing and FE analysis;
- treatment of NiTi wires, experimental damping characterization, and modeling of its behavior;
- fabrication process of the horn as laminated composite;
- simulation of the dynamic response of the horn;

This article is an invited paper selected from presentations at Shape Memory and Superelastic Technologies 2008, held September 21-25, 2008, in Stresa, Italy, and has been expanded from the original presentation.

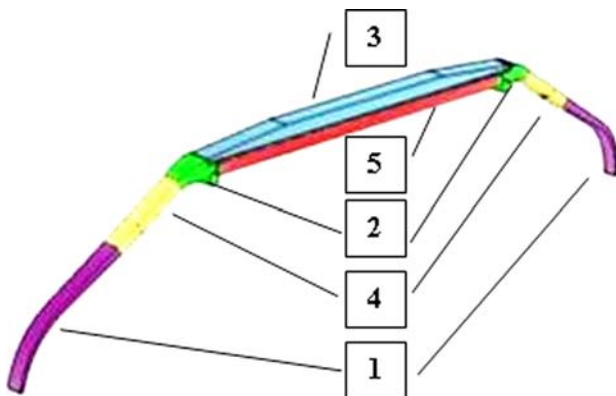
A. Tuissi, P. Bassani, and R. Casati, CNR, IENI, Unità di Lecco, Corso Promessi Sposi 29, 23900 Lecco, Italy; and M. Boccione, A. Collina, M. Carnevale, A. Lo Conte, and B. Previtali, Dipartimento di Meccanica, Politecnico di Milano, Via La Masa 1, 20156 Milano, Italy. Contact e-mail: andrea.collina@polimi.it.



**Fig. 1** Contribution of deformable collector modes to the spectrum of the contact force related to the effect of incident flow: wind tunnel measurement results



**Fig. 2** High-speed pantograph in contact with the catenary



**Fig. 3** Finite element model of the collector A: different parts are shown in colors (refer to Table 2)

- dynamic testing of the horn;
- remarks and future activities.

## 2. Modal Analysis of the Current Collector


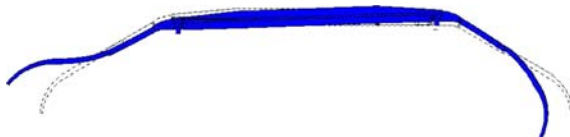
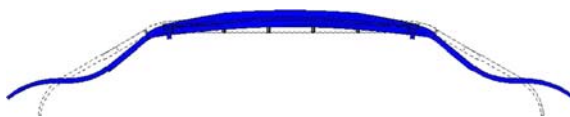
When considering current collectors for high-speed pantographs (see Fig. 2), common feature can be found in their structure. A current collector of a pantograph is composed at least of the following parts:

- one or two contact strips (copper or graphite or graphite with copper powder) that have the function of a sliding contact for collecting the current from the overhead line. This is the part that undergoes wear during the normal operation and excessive wear in case of arcing and continuous sparking;
- a steel or aluminum supporting structure for each contact strip (or couple of contact strip) that has a structural function and is connected to the articulated frame of the pantograph through the suspensions of the collector;
- lateral horns, whose function is to prevent the contact wire sliding under the collector, that are realized with polymeric material or fiber glass.

Analyzing the dynamic behavior of a collector, it can be found that low damped flexural modes of the collector are present starting from 50 Hz. In order to evaluate which components are more suitable for introducing damping, a FE model of the current collector has been set-up, able to reproduce the experimentally observed frequencies and mode shapes (Fig. 3 and Table 1). Hexahedral elements (C3D8R) with reduced integration have been used to the solid parts (contact strip, connecting blocks, and lateral horns), whereas quadrangular elements (S4R) have been adopted for the tubular parts (central supporting beams and lateral tubular beams). The contact between the different parts has been reproduced forcing the congruence between the surfaces of adjacent parts.

The model has been validated by means of the comparison with the experimental results from forced frequency response and impact tests. It can be observed that the maximum

**Table 1** Results of the FE analysis and comparison with experimental data for the collector

Mode no.	FE calculated mode shape	Exp. freq., Hz	FE freq., Hz
1		60.1	60
2		76.9	76.2
3		136	136

amplitudes occur in correspondence of the horns that play an important role in the location of the first flexural frequencies of the collector.

Analyzing the modal shape of the flexural modes, it can be shown that the horns contribute with a significant portion, from 42% up to 70% of the total strain energy associated to the first modes, as reported in Table 2.

For this reason it is proposed to use the horns as elements to increase the damping of the entire collector. The implementation of horns with laminated composite does not modify the structure of the collector; therefore, it can be easily implemented in the current design without need of architectural modification, and eventually proposed for a retrofit of the existing collectors.

### 3. NiTi Wires Realization, Characterization, and Modeling

As is known, NiTi alloys are characterized by a transformation between an austenitic phase B2 stable at high temperature and a martensitic B19' at low temperature. The corresponding characteristic temperatures can be properly set

**Table 2** Fraction of elastic energy distribution for the ATR95 FE calculated modes

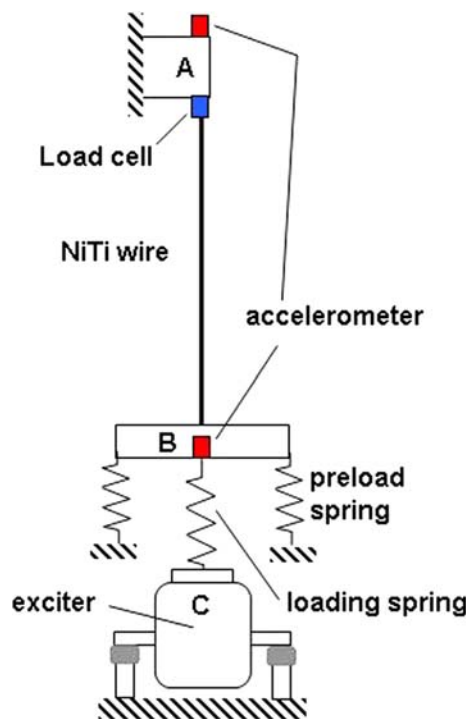
Parts of the collector	Color legend	Mode no.		
		1	2	3
Horns	1	0.46	0.7	0.42
Connecting bloks	2	0.13	0.09	0.05
Graphite strip	3	0.12	0.02	0.26
Lateral tubular beams	4	0.16	0.16	0.01
Central beam	5	0.13	0.03	0.26
Total		1	1	1

The color legend of Fig. 3 is recalled to distinguish the different parts

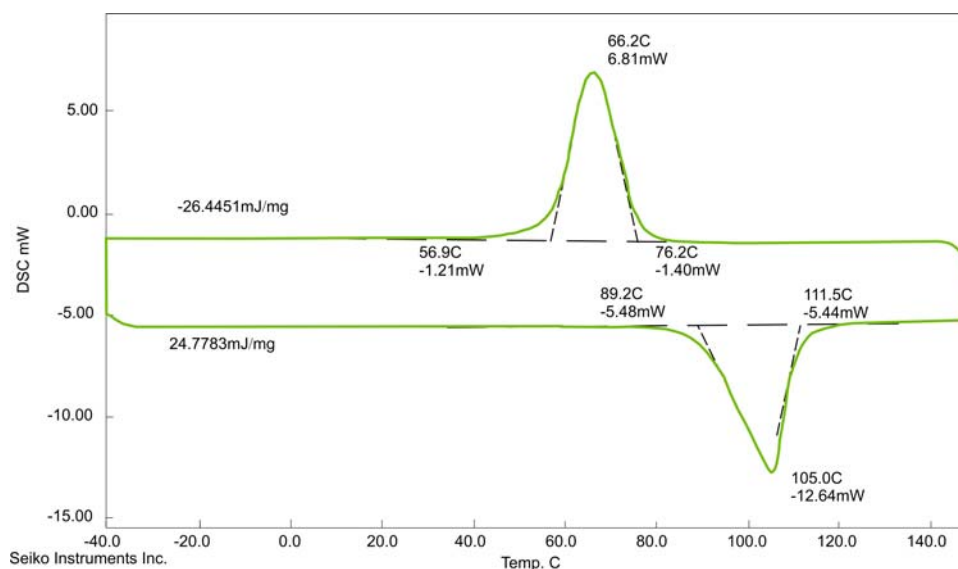
both through modifications of their composition and thermo-mechanical treatments.

In the literature it is well documented that the martensite of NiTi shows a damping capacity of at least an order of magnitude higher than classic structural metallic materials properties (Ref 5, 6).

Considering the expected low strain level of the application and the service temperature, it has been decided to use Ni<sub>49</sub>Ti<sub>51</sub> (at.%) alloy in order to have a martensitic temperature range below 90 °C. The material was melted by VIM furnace in a controlled argon atmosphere. The ingot was hot forged, hot



**Fig. 5** Sketch of the experimental set-up



**Fig. 4** DSC analysis of the NiTi wire material

rolled, and cold drawn down to 0.5 mm in diameter and then heat treated at 700 °C for 20 min in order to obtain an  $A_s$  of 90 °C as shown in the calorimetric curve (Fig. 4), from which the characteristic temperatures can be inferred:  $M_f$  56.9 °C,  $M_s$  76.2 °C,  $A_s$  90 °C, and  $A_f$  111.5 °C.

In order to determine the damping properties of the NiTi wires, ordinary vibration tests at ambient temperature in the frequency range 50-150 Hz have been carried out. The sketch of Fig. 5 shows the principle of the test set-up: the upper end of the wire is fixed and connected to a piezoelectric load cell, while the lower end is connected to an electro-dynamic shaker through a soft spring, in order to decouple the wire from the actuator. The wire is preloaded by a couple of springs. Accelerometers are placed in both extremities of the wire connections in order to measure the relative elongation of the wire, eliminating the effect of the residual vibration of the upper fixation point, which is connected to a supporting structure placed above the shaker. Since the forces that are involved are very low, a particular attention was devoted to the implementation of the set-up. In particular, the use of piezo-load cells has been preferred with respect to extensimetric ones in order to enhance the stiffness of the connecting point.

The tests have been carried out applying a sinusoidal waveform at 60 Hz, corresponding to the frequency of the first flexural mode of the collector of the pantograph for which the application is conceived. The range of deformations that have been investigated are between  $0.5 \times 10^{-4}$  and  $10^{-3}$ . The parameter  $\tan \delta$  is defined as:

$$\tan \delta = \frac{Im(\overline{F}/\overline{X})}{Re(\overline{F}/\overline{X})} \quad (\text{Eq 1})$$

In Eq 1  $\overline{F}$  is the complex number that represents the force at the test frequency, whereas  $\overline{X}$  is the complex number representing the amplitude of the relative motion of wire extremities. Figure 6 reports the parameter  $\tan \delta$  at 60 Hz as a function of the axial deformation of the wire. The latter is calculated through the difference of the acceleration of wire extremities, obtaining the relative displacements. Every point represents the results of each single test. Since the damping parameter is based on the phase difference between force and mobility signal, it is fundamental to detect the presence of eventual spurious effects due to the measurement chain, associated to the dynamic response of the transducers and the acquisition data system. An inertial test with the accelerometer placed on a calibrated mass, compared with the measurement of the load cell mounted under the mass, has been performed. The frequency response function between the load cell signal and the accelerometer signal is obviously expected

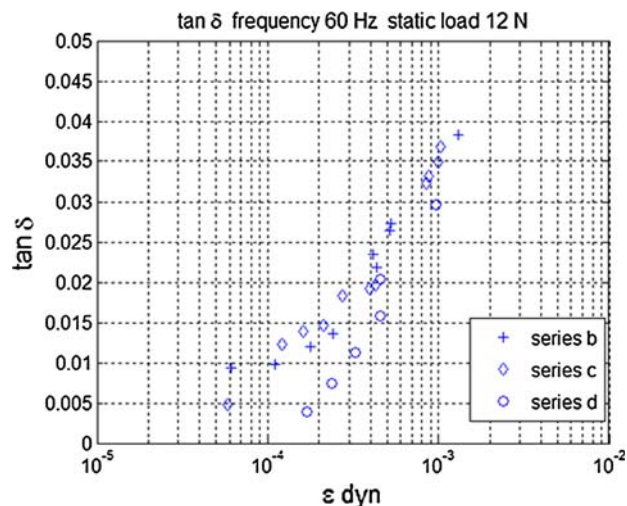


Fig. 6 Values of  $\tan \delta$  for the tested NiTi wires at preload of 12 N

The results obtained from the tests on the NiTi wires showed an amplitude dependence of the damping capacity, expressed as  $\tan \delta$  (see Fig. 6). Using the data obtained from the above-mentioned tests, a simple model has been developed to reproduce the dependence of the  $\tan \delta$  parameter on the strain amplitude.

State-of-the-art modeling of SMA focuses on the evolution of austenite-martensite transformation, through thermo-mechanical model (see, for instance, Ref 7, 8), for strain values of the order of 1%÷5%, including strain-rate dependence for low frequency. As mentioned earlier, in the present application lower strain amplitudes are induced, and the intrinsic damping of the martensite due to twin boundary movement is exploited.

For the purpose of phenomenological modeling of the damping of the examined wires, a friction-type model is adopted, following the definitions given in Ref 9. Different elementary hysteresis elements are combined in parallel, giving the non-linear strain amplitude dependence of the damping (Fig. 7). In addition, a fraction of the linear-dependent portion of damping is added with a viscous element. The identification is carried out following a procedure similar to the one described in Ref 10 for a related problem.  $(\sigma_i, \varepsilon_i)$  are the  $n$  points of the experimental stress-strain cycle, with strain amplitude  $A$ , used for the identification procedure. Equating the stress variation  $(\sigma_{i-1} - \sigma_i)$  across the  $(\varepsilon_{i-1} - \varepsilon_i)$  intervals to the stress variation obtained by the model used to reconstruct the stress-strain cycle, the following equation holds:

$$\begin{bmatrix} (\varepsilon_1 - \varepsilon_0)E_1 & 0 & \dots & 0 \\ (\varepsilon_1 - \varepsilon_0)E_1 & (\varepsilon_2 - \varepsilon_1)(E_1 + E_2) & \dots & 0 \\ \dots & \dots & \dots & 0 \\ (\varepsilon_1 - \varepsilon_0)E_1 & (\varepsilon_2 - \varepsilon_1)(E_1 + E_2) & \dots & (\varepsilon_n - \varepsilon_{n-1})(E_1 + E_2 + \dots + E_n) \end{bmatrix} + \begin{bmatrix} \sigma_{V,1} - \sigma_{V,0} \\ \sigma_{V,2} - \sigma_{V,1} \\ \dots \\ \sigma_{V,n} - \sigma_{V,n-1} \end{bmatrix} = \begin{bmatrix} \sigma_1 - \sigma_0 \\ \sigma_2 - \sigma_1 \\ \dots \\ \sigma_n - \sigma_{n-1} \end{bmatrix} \quad (\text{Eq 2})$$

to be the value of the mass, with a zero phase lag, but as a matter of fact a phase lag introduced by instrumentation has been found. The estimated instrumental phase lag at 60 Hz, equal to  $2^\circ 25'$ , is then subtracted from the phase lag value measured in the test on the wires.

where  $\sigma_{V_i}$  are the viscous contributions, which are set a priori considering the  $\tan \delta$  value of the lowest strain amplitude. From the previous expression the  $E_i$  unknowns can be calculated, while the limiting equivalent stress for each element  $\sigma_{ci}$  can be simply calculated as



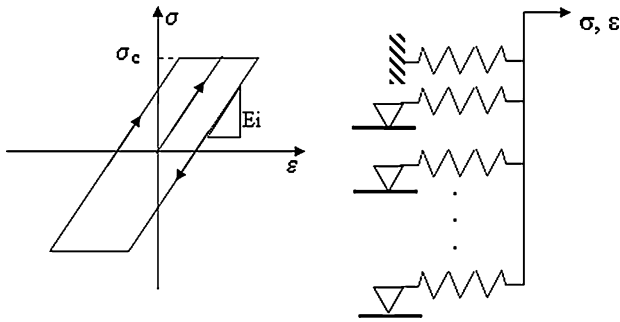


Fig. 7 Basic hysteresis model and combined in parallel used for the simulation of material behavior

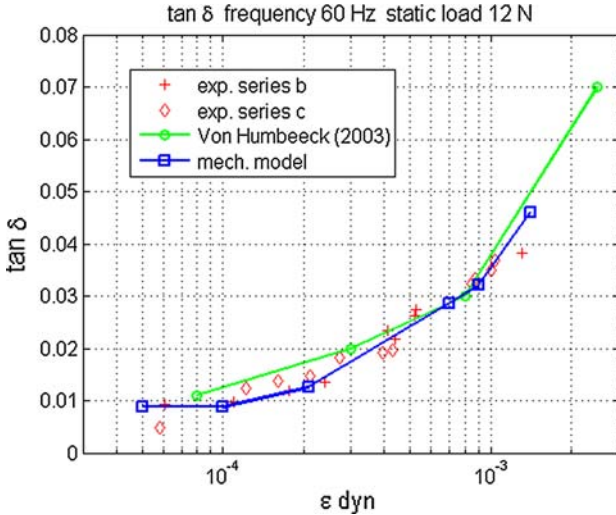


Fig. 8 Comparison of  $\tan \delta$  values obtained from the model with the measured ones as a function of strain amplitude

$$\sigma_{ci} = \frac{1}{2} E_i (A - \epsilon_i) \quad i = 2, n \quad (\text{Eq } 3)$$

In the presented application,  $n = 6$ .

The identification of the parameters  $E_i$  and  $\sigma_{ci}$  is carried out considering the stress-strain amplitude at the highest strain amplitude ( $1.4 \times 10^{-3}$ ). The model is then applied for the simulation of the behavior at lower strain amplitudes. From the stress-strain loop simulated at each amplitude, the corresponding  $\tan \delta$  values are calculated. Figure 8 shows the dependence of  $\tan \delta$  on the strain amplitude, compared with the measured results and with the values from Ref 5 in the same strain amplitude, although for a lower annealing temperature. The adopted modeling refers obviously to a constant ambient temperature since it does not include any temperature effect.

#### 4. Fabrication Process of the Laminated Composite and the Horn

As mentioned earlier, the proposed laminated composite consists of two external and one internal mat. The two external mats are two composite mats made by NiTi wires and epoxy fiberglass fabric, while the internal mat is made of epoxy fiberglass fabric. The outer surfaces of the composite mats are then covered by two epoxy fiberglass layers (see Fig. 9 and Table 3).

The fabrication process is divided into two steps. First, the fabrication of the composite mat having the horn shape is carried out using a metallic sheet in order to give the horn curvature. In particular, the first epoxy fiberglass fabric is positioned on the tool, the series of 13 NiTi wires are lined above the fabric and the second fiberglass fabric covers the NiTi wires (Fig. 10). Then, the eventual air bubbles are eliminated making use of a vacuum bag and the composite mat is cured in autoclave.

In the second step, the laminated composite is assembled, joining the two composite mats with NiTi wires with the inner part in epoxy fiberglass and adding the two external clad layers. In particular, the horn mold is filled with one epoxy fiberglass layer, the lower composite mat, about 30 layers of epoxy fiberglass fabric, the upper composite mat, and one final epoxy fiberglass layer.

After the cure cycle in autoclave the “horn” is finished as shown in Fig. 11.

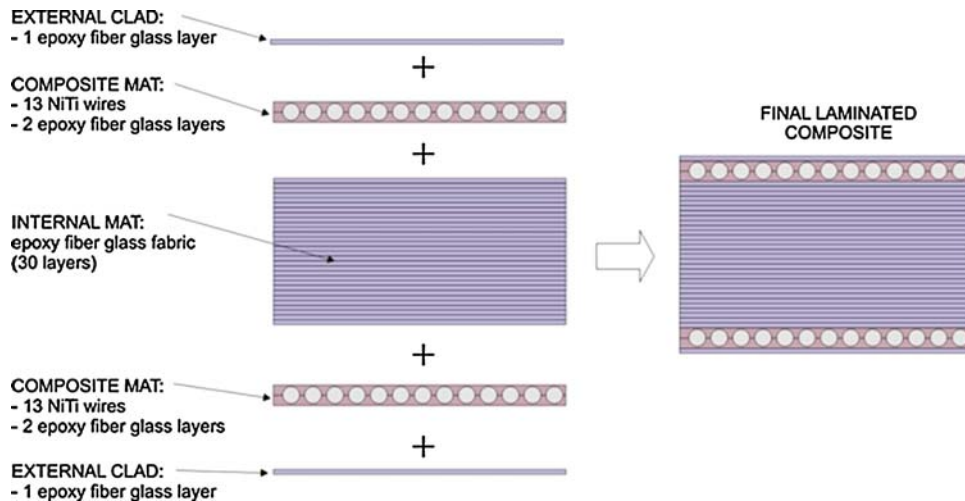
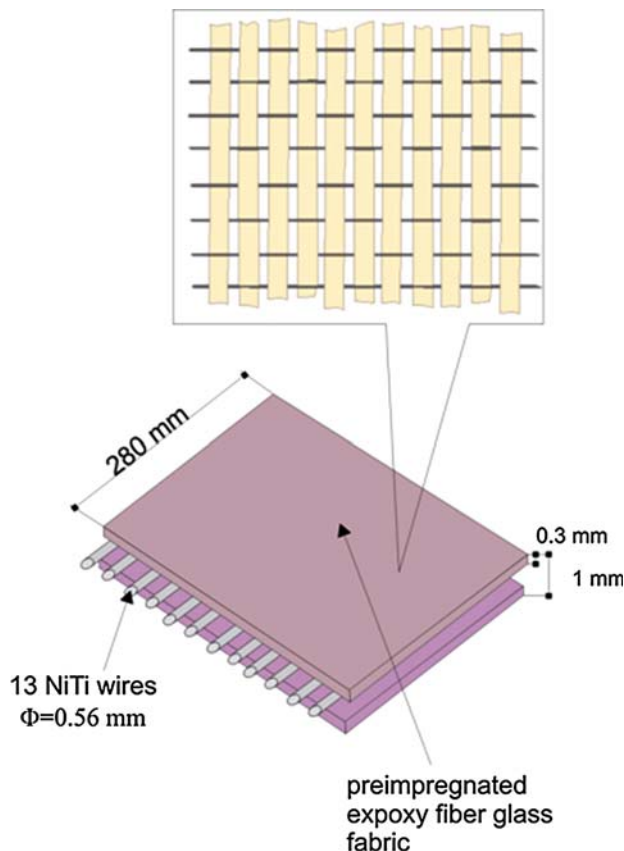


Fig. 9 Cross section of the laminated composite

**Table 3 Characteristic of the matrix**

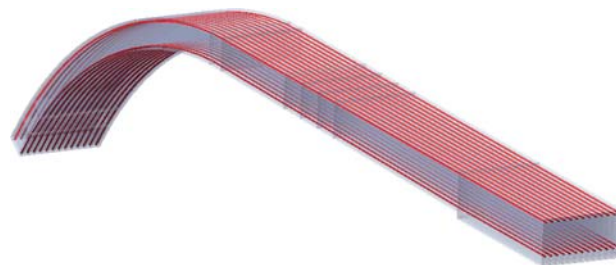
Matrix	Epoxy resin
Fiber	Glass EC9 5x136 tex (weft) Glass EC9 68 tex (warp)
Resin content	32%
Cure temperature	120 °C
Autoclave pressure	6 bar
Autoclave time	6 h

**Fig. 11** Final appearance of the horn in laminated composite**Fig. 10** Structure of the external mat

With the same procedure a laminated horn of only epoxy fiberglass has been fabricated, substituting the NiTi wires in the two external mats with two additional layers of epoxy fiberglass fabric, in order for the two horns to have the same height. The improvement due to NiTi wires in the composite horn has been established by comparison as shown in the following.

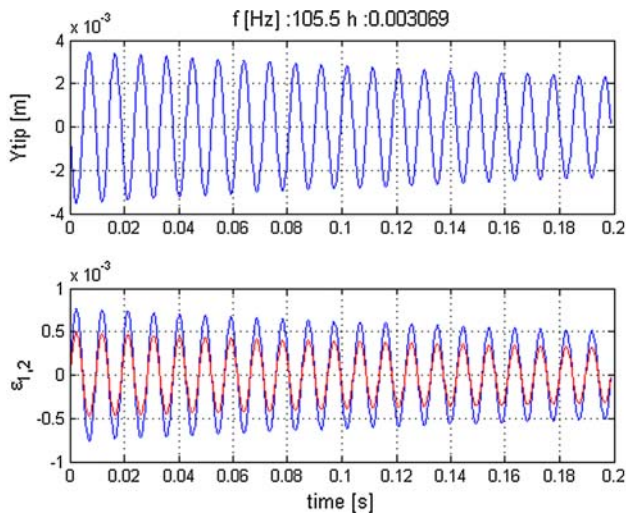
## 5. Finite Element Model of the Horn

A FE model of the horn fitted with the wires has been implemented in order to perform the dynamic analysis including the behavior of the material by means of the material behavior model previously presented. In Fig. 12, the FE model representing the horn and including the NiTi wires is shown corresponding to the prototype horn made as described previously. In the dynamic simulation, the horn is clamped at one extremity, and the initial excitation is a velocity field corresponding to the first flexural mode, so that the dynamic response reproduces a decay after an impulse application.

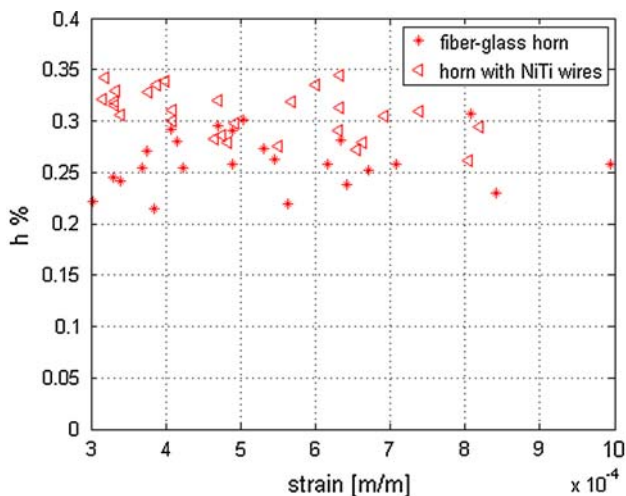
**Fig. 12** Finite element modeling of the horn, including the NiTi wires**Table 4** Results of the simulation of decay test

Configuration	Strain amplitude max	Frequency, Hz	Non-dimensional damping, %
Fiberglass only	...	101.4	0.27
NiTi 13 wires	$0.5 \times 10^{-3}$	105.5	0.298
	$0.75 \times 10^{-3}$	105.5	0.304
	$1 \times 10^{-3}$	105.5	0.336
	$1.25 \times 10^{-3}$	105.5	0.372
NiTi 20 wires	$0.5 \times 10^{-3}$	109.9	0.319
	$0.75 \times 10^{-3}$	109.9	0.329
	$1 \times 10^{-3}$	109.9	0.37
	$1.25 \times 10^{-3}$	109.9	0.419

Based on a DMTA analysis, the fiberglass material characteristics are assumed as follows: Young modulus  $1.82 \times 10^{10}$  Pa, with a non-dimensional damping  $h = 0.0027$  associated to the first flexural mode. The behavior of the NiTi wires is included as a user-defined subroutine for the related material, with the actual strain condition as input and the corresponding stress in output. In this way, the strain dependence of the model accounts for the different values of strain along the horn for flexural vibrations. Moreover, different values of the vibration and consequently different strain amplitudes are considered in order to verify the dependence of the NiTi modeling included in the FE calculation. Table 4 reports the results in terms of non-dimensional damping obtained respectively for the matrix material only for the configuration with 13 wires for each of the two external mat (corresponding to the real prototype) and with a configuration with 20 wires for each external mat. The non-dimensional damping  $h\%$ , calculated from the logarithmic decrement (see Fig. 13), increases with amplitude of the strain, as expected from the model adopted for the SMA. Simulated values of  $h\%$  damping are in the range from 0.27%, related to the fiberglass matrix alone, up to 0.37%, at the maximum amplitude in the configuration with 13 NiTi alloy wires.



**Fig. 13** Simulated decay. Upper graph: motion at the tip of the horn (with NiTi wires) in the vertical direction. Lower graph: strain in the section at 30 and 110 mm from the clamped section



**Fig. 14** Comparison of experimental non-dimensional damping ( $r/rc$ ) related to the first flexural frequency obtained from the decay response test on fiberglass only and NiTi composite horns

A secondary effect of the NiTi wires is that the flexural frequency increases with the number of wires, indicating the influence of the higher stiffness of the wires.

## 6. Dynamic Testing of the Horn

Experimental decay tests have been carried out in a single cantilever configuration on both the fabricated horns (epoxy fiberglass with NiTi wires and only epoxy fiberglass), in order to identify the non-dimensional damping values related to their first flexural mode. The horns have been given an initial displacement condition and the decay response has been measured by means of a triangulation laser MEL model M5L/10 pointing at a distance of 155 mm from the clamp. The

laser sensor was used in order to provide a non-contact measurement. Strains at the distance of 30 and 170 mm from the clamp have been measured by means of strain gages in a half bridge configuration.

The results of experimental non-dimensional damping  $h = r/rc$  associated to the first flexural mode, calculated from the logarithmic decrement over five periods, are reported in Fig. 14 for both the horns, as a function of the mean strain amplitude of the analyzed periods, measured at the distance of 30 mm from the clamp. Due to epoxy fiberglass initial values of  $\tan \delta$  0.54% and to  $\tan \delta$  dependence on strain for the NiTi wires (Fig. 6), damping improvement can be expected when strains along the horn are higher than  $1E-4$ . The mean value of the non-dimensional damping  $h$  for experimental data has increased from 0.0027 in the case of fiberglass laminated horn to the value of 0.003 for the horn containing NiTi wires, which means an increase of 11% in the non-dimensional damping of the first flexural mode.

## 7. Conclusions

A composite material made with fiberglass mats and NiTi wires has been proposed for an application on the current collector for pantographs, with the aim of increasing its damping capacity related to the first flexural mode, keeping the original configuration, and therefore without any need of structural modification in the architecture of the collector.

The developed NiTi wires have been produced and dynamically tested at 60 Hz for the determination of damping parameter  $\tan \delta$ . According to the obtained results, a simple phenomenological model with strain amplitude dependence has been developed and applied to the simulation of a FE model of the horn.

A first prototype of the horn has been made too in order to assess its fabrication process, and it has been tested dynamically in laboratory. NiTi wires collaborate in the composites since the experimental data obtained for non-dimensional damping  $h$  of the first flexional mode increase of 11%.

## Acknowledgment

The authors thank Mako Shark S.r.l-Viale Montecuccoli 18, 23843 Dolzago (LC), Italy, for the realization of the laminated horns.

## References

1. M. Bocciolone, A. Collina, A. Lo Conte, B. Previtali, A. Tuissi, and P. Bassani, Characterisation and Modeling of a Shape Memory Material for the Increase of the Structural Damping of Collectors for High Speed Pantographs, XXXV Convegno Nazionale AIAS, 13–16 Settembre 2006, Università Politecnica delle Marche (in italian)
2. R. Zhang, Q.-Q. Ni, A. Masuda, T. Yamamura, and M. Iwamoto, Vibration Characteristics of Laminated Composite Plates with Embedded Shape Memory Alloys, *Compos. Struct.*, 2006, **74**, p 389–398
3. K.-t. Lau, L.-m. Zhou, and X.-M. Tao, Control of Natural Frequencies of a Clamped–Clamped Composite Beam with Embedded Shape Memory Alloy Wires, *Compos. Struct.*, 2002, **58**, p 39–47
4. Y. Matsuzaki, T. Ikeda, and C. Boller, Technological Development of Passive and Active Vibration Control: Analysis and Test, *Smart Mater. Struct.*, 2005, **14**, p 343–348

5. J. Van Humbeeck, Damping Capacity of Thermoelastic Martensite in Shape Memory Alloys, *J. Alloys Compd.*, 2003, **355**, p 58–64
6. S.K. Wua and H.C. Lin, Damping Characteristics of TiNi Binary and Ternary Shape Memory Alloys, *J. Alloys Compd.*, 2003, **355**, p 72–78
7. F. Auricchio, D. Fugazza, and R. Des Roches, Numerical and Experimental Evaluation of the Damping Properties of Shape-Memory Alloys, *ASME J. Eng. Mater. Technol.*, 2006, **128**, p 312–319
8. T. Ikeda, F.A. Nae, H. Naito, and Y. Matsuzaki, Constitutive Model of Shape Memory Alloys for Unidirectional Loading Considering Inner Hysteresis Loops, *Smart Mater. Struct.*, 2004, **13**, p S916–S925
9. J. Van Humbeeck and S. Kustov, Active and Passive Damping of Noise and Vibrations Through Shape Memory Alloys: Applications and Mechanisms, *Smart Mater. Struct.*, 2005, **14**, p S171–S185
10. A. Falvo, F. Furgiuele, and C. Maletta, Hysteresis Modeling of Two-Way Shape Memory Effect in NiTi Alloys, *Meccanica*, 2008, **43**, p 165–172